

Article

# Safety-Guaranteed, Robust, Nonlinear, Path-Following Control of the Underactuated Hovercraft Based on FTESO

Mingyu Fu and Qiusu Wang \*

Department of Intelligent Systems Science and Engineering, Harbin Engineering University, Harbin 150006, China; fumingyu@hrbeu.edu.cn

\* Correspondence: 15261862656@163.com

**Abstract:** On account of the external disturbances and difficult maneuverability of a hovercraft, this paper devises a safety-guaranteed, robust, nonlinear, path-following control strategy of a hovercraft targeted for unknown dynamics, unavailable velocity, and unknown external ocean disturbances. Firstly, for the sake of accurately observing unavailable lumped disturbances and unavailable velocity measurements, a finite-time extended state observer (FTESO) is proposed. Secondly, a line-of-sight (LOS) guidance law constructed with a bounded-gain-forgetting (BGF) adaptive estimator is devised to follow the desired path while considering external environmental disturbances accurately, in which the tracking errors and the parameter estimation are both proven to be bounded. In addition, for the sake of safety, a safety-guaranteed auxiliary system that can constrain the drift angle during the hovercraft's navigation is proposed. Thirdly, the robust, nonlinear, path-following controllers achieved high tracking performance with the constructed safety-guaranteed compensation backstepping method. Finally, according to the Lyapunov and homogeneous theories, the observation error can be guaranteed to zero and the tracking error can converge to an arbitrarily small region near zero in finite time. Numerical simulations illustrate the effectiveness for the proposed robust, nonlinear, path-following scheme.

**Keywords:** hovercraft; path-following control; FTESO; line-of-sight



**Citation:** Fu, M.; Wang, Q. Safety-Guaranteed, Robust, Nonlinear, Path-Following Control of the Underactuated Hovercraft Based on FTESO. *J. Mar. Sci. Eng.* **2023**, *11*, 1235. <https://doi.org/10.3390/jmse11061235>

Academic Editor: Sergei Chernyi

Received: 10 May 2023

Revised: 5 June 2023

Accepted: 11 June 2023

Published: 15 June 2023



**Copyright:** © 2023 by the authors. Licensee MDPI, Basel, Switzerland. This article is an open access article distributed under the terms and conditions of the Creative Commons Attribution (CC BY) license (<https://creativecommons.org/licenses/by/4.0/>).

## 1. Introduction

The hovercraft's main actuators include a vertical air rudder mounted behind every propeller and two air propellers at the stern normally [1]. Hence, the hovercraft is a typical underactuated ship. A hovercraft, as depicted in Figure 1, can run above the water surface. A hovercraft is faster than normal displacement vessels because of its low hydrodynamic resistance. Hence, the hovercraft has increasingly attracted more attention in both civil and military domains due to its particular performance [2].

Obviously, when sailing at low speed, the hovercraft has poor stability for coursing. It is easy for a hovercraft to experience heeling motion during fast turning. The abovementioned issues highlight many safety challenges for a hovercraft. It is dangerous when the stern kick-off phenomenon happens, as it may result in the hovercraft capsizing at high speed [2]. In addition, regarding the detailed review of the available literature about a hovercraft's trajectory tracking control [3–8], only state feedback was taken into consideration, and the literature about the output feedback on a hovercraft combined with its unique characteristics are few.

Considered that a hovercraft is a typical underactuated ship, various control methods of the underactuated surface vessels can be referenced. To solve the above difficulties, in recent years, various control methods have been reported through researchers' efforts with remarkable success. Some robust control algorithms have been presented, subject to the high nonlinearity of underactuated surface vessels. In [9], for an underactuated ship aiming to follow the given route, an adaptive control law is proposed according to parameter

estimation and sliding mode theory. For the sake of enhancing strong robustness and reducing oscillation of the whole control system with unavailable parameters and external environmental disturbances, an adaptive continuous sliding mode scheme is designed. In [10], constructed with the disturbance observer, a new robust formation control law via the minimal learning parameter algorithm is presented. In [11], an accurate, safety-guaranteed, area-keeping control scheme for an unmanned surface vessel is proposed that illustrates the safety and stability during the whole control. In [12], a coordinated tracking problem is considered for unmanned surface vehicles (USV) with communication delays and constrained actuation resources. Its position can be obtained by a small fraction of USVs, whereas its velocity is not available to follower USVs. An adaptive control law for path following of an unmanned surface vehicle based on deep reinforcement learning theory is proposed in [13]. The presented controller is capable of following the given path via interacting with the nearby environment.



**Figure 1.** The underactuated hovercraft.

Although the aforementioned research has good effectiveness for unknown uncertainties and external disturbances, the aforementioned control laws only consider state feedback; in other words, all ship signals are required to be known. Actually, because of the hull space and equipment cost limitation, the hovercraft is not allocated with a speed sensor or noise contamination sensor. During feedback control, a vessel's velocity is unavailable. Therefore, the robust path-following control strategy is significant for the motion of a hovercraft. Unfortunately, few studies have been carried out with regard to the underactuated hovercraft. In [14], an attitude tracking control approach developed for the nonlinear quadrotor model guarantees the desired performance within finite time reliably. Via delay-dependent Lyapunov functional theory, the annular finite-time filters are devised and the filtering error system (FES) is illustrated to attenuate the environmental disturbances with high performance in [15]. Combined with the observer of strict-feedback nonlinear systems that observing the environmental disturbance and fuzzy approximation errors in finite time, an event-triggered fuzzy control strategy based on an adaptive technique is presented in [16] with strong robustness.

Combined with the adaptive fuzzy technique, Ref. [17] illustrates a control strategy that can follow a programmed path for underactuated vessels and achieves good tracking performance. In [18], considering surge-heading guidance, a path-following control scheme is devised. Unfortunately, these studies only consider state feedback and the unavailable velocity is ignored in [17–19]. In [20], a new FTESO is designed to observe the unavailable velocity and disturbances with good accuracy. The LOS guidance approach, which is based on velocity observations, is introduced to obtain the reference yaw law. In [21], the output feedback control laws are proposed to follow the programmed path precisely with tracking performance in finite time.

Nevertheless, it is noted that research on finite-time motion control for a hovercraft is a challenge on account of the real hovercraft’s sailing characteristics. Although the finite-time theories have good convergence performance and precision characteristics, there are few pieces of research with regard to path-following control for a hovercraft.

Motivated by the aforementioned analysis, this paper is targeted to resolve the robust, nonlinear, path-following control problem for the hovercraft with regard to the unavailable velocity measurement and unavailable external disturbances. Firstly, for the sake of observing total compound disturbances, an FTESO is devised. Secondly, based on the bounded-gain-forgetting (BGF) estimator and adaptive technique, a line-of-sight (LOS) guidance law is developed to track the programmed path with good accuracy, in which errors are bounded. Thirdly, for sake of safety, a safety-guaranteed auxiliary system that can restrain the drift angle in real-time is developed. Subsequently, because of the actuators’ natural capabilities, robust, nonlinear control laws are established to follow the programmed path with the constrained control input. Finally, it can be illustrated that the designed safety-guaranteed, robust, nonlinear, path-following control strategy can ensure that the errors converge to near zero precisely and all signals are bounded in finite time. The main characteristics of the paper are generalized as follows:

(1) Considering the real hovercraft’s motion characteristics, the FTESO is used for path following of the underactuated hovercraft. The estimation errors are proved to converge to zero accurately via homogeneous theories, and the FTESO enhances the whole system’s robustness.

(2) The reference yaw angle, which is proposed by a LOS guidance law based on the BGF adaptive estimator (BGF-LOS), can guarantee the performance of decreasing the convergence time.

(3) Aiming at safe navigation of the hovercraft, the constructed safety-guaranteed, robust, nonlinear control strategy possesses two advantages, which are its stronger, robust anti-interference ability and higher precision performance.

The rest of the paper is organized as follows. The preliminary, subsequently required standards and assumptions are introduced in Section 2. The reference yaw angle and the safety-guaranteed, robust, nonlinear, path-following control scheme based on FTESO are discussed in Section 3. Stability analysis is proposed in Section 4. Numerical simulations that demonstrate the feasibility and universality of the proposed control law are given in Section 5. Lastly, conclusions are shown in Section 6.

## 2. Preliminaries and Problem Formation

### 2.1. Preliminaries

**Definition 1** ([22]). For a vector  $\mathbf{x} = [x_1, x_2, \dots, x_n]^T \in \mathbf{R}^n$ , a continuous function  $g(\mathbf{x}): \mathbf{R}^n \rightarrow \mathbf{R}$  is homogeneous with degree  $k$  with respect to the dilation.  $(\lambda^{r_1}x_1, \lambda^{r_2}x_2, \dots, \lambda^{r_n}x_n)$ , if  $g(\lambda^{r_1}x_1, \lambda^{r_2}x_2, \dots, \lambda^{r_n}x_n) = \lambda^k g(\mathbf{x}), \forall \lambda > 0$ , where  $k > -\min\{r_i\}, (i = 1, 2, \dots, n)$ .  $\dot{\mathbf{x}} = \mathbf{g}(\mathbf{x})$  (or a vector  $\mathbf{g}$ ) is a differential system with continuous:  $\mathbf{g}(\mathbf{x}) : \mathbf{R}^n \rightarrow \mathbf{R}$  is homogeneous with degree  $k$  with regard to the dilation  $(\lambda^{r_1}x_1, \lambda^{r_2}x_2, \dots, \lambda^{r_n}x_n)$ ; if  $g(\lambda^{r_1}x_1, \lambda^{r_2}x_2, \dots, \lambda^{r_n}x_n) = \lambda^k g(\mathbf{x}), \forall \lambda > 0$ .

**Lemma 1** ([23]). Suppose that there is a positive, definite, continuous Lyapunov function  $V(\mathbf{x}, t)$  defined on  $\mathbf{U}_1 \in \mathbf{R}^n$  of the origin and

$$\dot{V}(\mathbf{x}, t) < -c_1 V^\alpha(\mathbf{x}, t) + c_2 V(\mathbf{x}, t), \forall \mathbf{x} \in \mathbf{U}_1 \setminus \{0\} \tag{1}$$

where  $c_1 > 0, c_2 > 0$ , and  $0 < \alpha < 1$ . Thus, the origin of system (1) is locally finite-time stable. The set  $\mathbf{U}_2 = \{\mathbf{x} | V^{1-\alpha}(\mathbf{x}, t) \leq c_1/c_2\}$  is contained in the domain of attraction of the origin. The settling time satisfies  $T \leq \ln(1 - (c_2/c_1)V^{1-\alpha}(\mathbf{x}_0, t_0))/(c_2\alpha - c_2)$  for a given  $\mathbf{x}(t_0) \in \{\mathbf{U}_1 \cap \mathbf{U}_2\}$ .

**Lemma 2** ([24]). For  $\forall x_i \in \mathbf{R}, i = 1, \dots, n, 0 \leq q < 1$ ; then,

$$\left(\sum_{i=1}^n |x_i|\right)^q \leq \sum_{i=1}^n |x_i|^q \leq n^{1-q} \left(\sum_{i=1}^n |x_i|\right)^q \tag{2}$$

**Lemma 3** ([25]). For  $\forall x_i \in \mathbf{R}, i = 1, \dots, n$ , and a real number  $p > 1$ ,

$$\sum_{i=1}^n |x_i|^p \leq \left(\sum_{i=1}^n |x_i|\right)^p \leq n^{p-1} \sum_{i=1}^n |x_i|^p \tag{3}$$

2.2. Model of Underactuated Hovercraft

The three-DOF hovercraft model is as follows:

$$\begin{aligned} \begin{pmatrix} \dot{x} & \dot{y} & \dot{\psi} \end{pmatrix}^T &= S(\psi) \begin{pmatrix} u & v & r \end{pmatrix}^T \\ \begin{pmatrix} \dot{u} \\ \dot{v} \\ \dot{r} \end{pmatrix} &= \begin{pmatrix} vr \\ -ur \\ 0 \end{pmatrix} + M \begin{pmatrix} R_u + \tau_u \\ R_v \\ R_r + \tau_r \end{pmatrix} \end{aligned} \tag{4}$$

where

$$\begin{aligned} S(\psi) &= \begin{pmatrix} \cos \psi & -\sin \psi & 0 \\ \sin \psi & \cos \psi & 0 \\ 0 & 0 & 1 \end{pmatrix} \\ M &= \begin{pmatrix} \frac{1}{m} & 0 & 0 \\ 0 & \frac{1}{m} & 0 \\ 0 & 0 & \frac{1}{J_z} \end{pmatrix} \end{aligned} \tag{5}$$

The signals  $u, v, r$  are the surge and sway velocities, and the turning rate, respectively;  $x, y$  represent the hovercraft's position in the earth fixed frame;  $\psi$  describes yaw angle;  $m$  and  $J_z$  are the hovercraft's mass and moments of inertia;  $\tau_u$  and  $\tau_r$  are the control inputs. The total drags of the known model are denoted by  $R_m, R_{wm}, R_{sk}, R_u, R_v, R_r$ . For  $p_c, S_c, (R_u \ R_v \ R_r)^T$ , please refer to [1,3,26] to obtain more details.

In Figure 2, we obtain

$$v = u \tan \beta \tag{6}$$

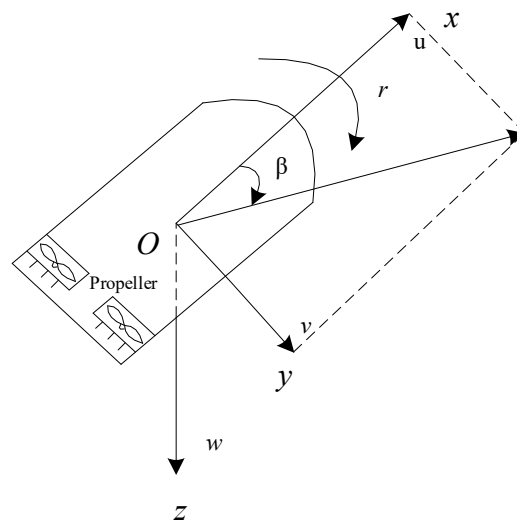


**Figure 2.** Diagram of the underactuated hovercraft.

For the sake of more convenience for controlling  $\beta$ , an improved model is derived from (4) and (6)—that is,

$$\begin{aligned} \begin{pmatrix} \dot{x} & \dot{y} & \dot{\psi} \end{pmatrix}^T &= S(\psi) \begin{pmatrix} u & u \tan \beta & r \end{pmatrix}^T \\ \begin{pmatrix} \dot{u} \\ \dot{v} \\ \dot{r} \end{pmatrix} &= \begin{pmatrix} ur \tan \beta \\ -\frac{u \sin(2\beta)}{2u} - r \cos^2 \beta \\ 0 \end{pmatrix} + M \begin{pmatrix} R_u + \tau_u \\ R_v \frac{\cos^2 \beta}{u} \\ R_r + \tau_r \end{pmatrix} \end{aligned} \tag{7}$$

**Assumption 1 ([1]).**

(1) A hovercraft state satisfies  $u(0) > k_{Iu}(t)$ ,  $|v(0)| < k_{Rv}(t)$ ,  $|r(0)| < k_{Rr}(t)$ . The safety boundaries  $k_{Iu}(t)$ ,  $k_{Rv}(t)$ , and  $k_{Rr}(t)$  will be discussed later on.

(2) The hovercraft has two identical air propellers and two identical air rudders, which are symmetrically mounted on the tail of the hull; they can only be operated simultaneously, not separately.

**2.3. The Hovercraft Dynamics of Tracking Error**

The path-following depiction can be seen in Figure 3 below.

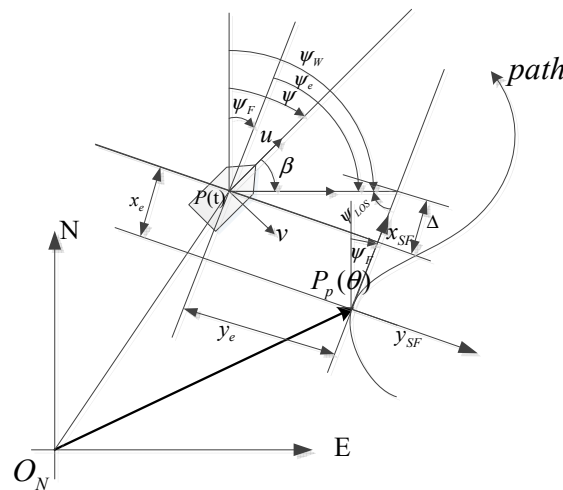


**Figure 3.** Path-following depiction of a hovercraft.

The above parameter as shown is represented by  $\vartheta$ . A Serret–Frenet (SF) system is introduced to obtain the error for path following. An arbitrary point  $P_F(\vartheta)$  is set in advance as the origin on the desired path.  $\psi_F(\vartheta) = a \tan 2(x'_F(\vartheta), y'_F(\vartheta))$ , where  $x'_F(\vartheta) = \partial(x'_F)/\partial\vartheta$  and  $y'_F(\vartheta) = \partial(y'_F)/\partial\vartheta$ .  $P(\vartheta) = (x, y)$  represents the hovercraft’s position, as depicted in Figure 3.  $P_F(\vartheta) = (x_F(\vartheta), y_F(\vartheta))$  is the position of the motional target point along the programmed path set in advance.

The error scheme In the SF system is depicted as follows:

$$\begin{bmatrix} x_e \\ y_e \end{bmatrix} = \begin{bmatrix} \cos \psi_F(\vartheta) & -\sin \psi_F(\vartheta) \\ \sin \psi_F(\vartheta) & \cos \psi_F(\vartheta) \end{bmatrix}^T \begin{bmatrix} x - x_F(\vartheta) \\ y - y_F(\vartheta) \end{bmatrix} \tag{8}$$

where  $x_e, y_e$  denote tracking errors.

Taking the derivative of Equation (13), the location tracking error dynamics can be obtained as follows:

$$\begin{bmatrix} \dot{x}_e \\ \dot{y}_e \end{bmatrix} = \begin{bmatrix} u \cos(\psi - \psi_F(\vartheta)) - v \sin(\psi - \psi_F(\vartheta)) + \dot{\psi}_F(\vartheta)y_e - \dot{\vartheta} \sqrt{x'^2_F(\vartheta) + y'^2_F(\vartheta)} \\ u \sin(\psi - \psi_F(\vartheta)) + v \cos(\psi - \psi_F(\vartheta)) - \dot{\psi}_F(\vartheta)x_e \end{bmatrix} \tag{9}$$

Considering the underactuated hovercraft model (4) and (5) in the presence of unavailable velocity and complex external disturbances, this paper aims to propel the hovercraft to follow the programmed path in finite time by developing the guidance law and safety-guaranteed, robust, nonlinear, path-following control strategy.

#### 2.4. Actuator Saturation Nonlinearity and State Constraints

Considering the practical application of a hovercraft, in view of the actuators' physical constraints, the control force can be expressed as follows:

$$\tau_i = \begin{cases} \tau_{i\max}, & \text{if } \tau_{ic} > \tau_{i\max} \\ \tau_{ic}, & \text{if } \tau_{ic} \leq \tau_{i\max} \\ \tau_{i\min}, & \text{if } \tau_{ic} < \tau_{i\min} \end{cases} \quad i = u, r \quad (10)$$

**Assumption 2.** All position, orientation, and acceleration values of a hovercraft are available for feedback.

The safety-guaranteed issue of  $\beta$  and the hump speed need to be obtained from model calculation and real vessel experience [2,27]. In this article, they are assumed to be the state constraint, which can be obtained. The safety constraint is defined as

$$\beta_{\min} \leq \beta \leq \beta_{\max} \quad (11)$$

### 3. Safety-Guaranteed, Robust, Nonlinear, Path-Following Control Strategy

#### 3.1. Design of Finite-Time Extended State Observer

Transform the 3-degrees of freedom hovercraft model (4) and (5) as follows:

$$\begin{aligned} \dot{\eta} &= S(\psi)v \\ M\dot{v} &= d + \tau + \tau_w \end{aligned} \quad (12)$$

where  $\tau = [\tau_u, 0, \tau_r]^T$ ,  $M = \text{diag}\{m, m, J_z\}$ ,  $\eta = [x, y, \psi]^T$ ,  $v = [u, v, r]^T$ , and  $\tau_w = [\tau_{uw}, \tau_{vw}, \tau_{rw}]^T$ .  $d = [d_u, d_v, d_r]^T$  denotes the model uncertainties, which are written as follows:  $d_u = m^{-1}ur \tan \beta + R_u$ ,  $d_v = m^{-1}(-\frac{\dot{u} \sin(2\beta)}{2u} - r \cos^2 \beta) + R_v$ ,  $d_r = R_r$ .

Aiming to draw forth the FTESO, set  $\mu = S(\psi)v$ , (12) can be obtained as follows:

$$\begin{aligned} \dot{\eta} &= \mu \\ \dot{\mu} &= d_1 + S(\psi)M^{-1}\tau \end{aligned} \quad (13)$$

where  $\mu = [\mu_u \ \mu_v \ \mu_r]^T$ ,  $d_1 = S(\psi)M^{-1}(\tau_w + d) + S(\psi)Rv$ ,  $R = \begin{pmatrix} 0 & -r & 0 \\ r & 0 & 0 \\ 0 & 0 & 0 \end{pmatrix}$ s.

**Assumption 3.** The rate of external disturbances  $d_1$  is unknown but bounded, which meets the next requirement  $\|\dot{d}_1\| \leq d_m$ , with  $d_m < \infty$  denoting a positive constant.

**Assumption 4.** The whole signals of a hovercraft are bounded, and a positive constant  $\epsilon$  and a compact set  $\Xi_1$ , where  $\Xi_1 = \{(\eta, \mu, \dot{\eta}, \dot{\mu}) \mid \|\eta\| < \epsilon, \|\mu\| < \epsilon, \|\dot{\eta}\| < \epsilon, \|\dot{\mu}\| < \epsilon\}$  can be found.

**Remark 3.** In a hovercraft's sail process,  $u, v, r$  of a hovercraft can be finite because of the hovercraft's performance containing air resistance constraints and a hydrodynamic damping term [28].

The FTESO of (12) is designed as follows:

$$\begin{aligned} \dot{\hat{\eta}} &= \hat{\mu} - l_1 \text{sig}^{m_1}(\tilde{\eta}) - \lambda_1 \text{sgn}(\tilde{\eta}) \\ \dot{\hat{\mu}} &= \hat{d}_1 + \mathbf{S}(\psi)\mathbf{M}^{-1}\boldsymbol{\tau} - l_2 \text{sig}^{m_2}(\tilde{\eta}) - \lambda_2 \text{sgn}(\tilde{\eta}) \\ \dot{\hat{d}}_1 &= -l_3 \text{sig}^{m_3}(\tilde{\eta}) - \lambda_3 \text{sgn}(\tilde{\eta}) \end{aligned} \tag{14}$$

where  $\hat{\eta}$ ,  $\hat{\mu}$ ,  $\hat{d}_1$  are the observations of  $\eta$ ,  $\mu$ ,  $d_1$ , respectively, and  $\tilde{\eta} = \hat{\eta} - \eta = [\tilde{\eta}_u \ \tilde{\eta}_v \ \tilde{\eta}_r]^T$ ,  $\tilde{\mu} = \hat{\mu} - \mu = [\tilde{\mu}_u \ \tilde{\mu}_v \ \tilde{\mu}_r]^T$ , and  $\tilde{d}_1 = \hat{d}_1 - d_1 = [\tilde{d}_u \ \tilde{d}_v \ \tilde{d}_r]^T$  are the FTESO observation errors,  $\frac{2}{3} < m_1 < 1, m_2 = 2m_1 - 1, m_3 = 3m_1 - 2, \text{sig}^{m_i}(\tilde{\eta}) = |\tilde{\eta}|^{m_i} \text{sgn}(\tilde{\eta}) (i = 1, 2, 3)$ . The parameters  $m_i (i = 1, 2, 3)$ ,  $l_i (i = 1, 2, 3)$ , and  $\lambda_i (i = 1, 2, 3)$  are positive definite coefficients, which can be set according to the Lyapunov functional theories and finite-time theories.

Combining (13) with (14), the error system is proposed as

$$\begin{aligned} \dot{\tilde{\eta}} &= \hat{\mu} - l_1 \text{sig}^{m_1}(\tilde{\eta}) - \lambda_1 \text{sgn}(\tilde{\eta}) \\ \dot{\tilde{\mu}} &= \hat{d}_1 - l_2 \text{sig}^{m_2}(\tilde{\eta}) - \lambda_2 \text{sgn}(\tilde{\eta}) \\ \dot{\tilde{d}}_1 &= -\hat{d}_1 - l_3 \text{sig}^{m_3}(\tilde{\eta}) - \lambda_3 \text{sgn}(\tilde{\eta}) \end{aligned} \tag{15}$$

The stability proof of (15) is to be provided later.

**Theorem 1.** For the hovercraft model described in (13) in the presence of the unknown dynamic and external disturbances, and unavailable velocity under Assumptions 1–4, the FTESO established in (14) is illustrated to estimate the external disturbance and the error can converge to zero within finite time.

**Proof of Theorem 1.** Firstly, omit the terms  $-\lambda_1 \text{sgn}(\tilde{\eta})$ ,  $-\lambda_2 \text{sgn}(\tilde{\eta})$ , and  $-\hat{d}_1 - \lambda_3 \text{sgn}(\tilde{\eta})$ , the error dynamics can be represented as

$$\begin{aligned} \dot{\tilde{\eta}} &= \hat{\mu} - l_1 \text{sig}^{m_1}(\tilde{\eta}) \\ \dot{\tilde{\mu}} &= \hat{d}_1 - l_2 \text{sig}^{m_2}(\tilde{\eta}) \\ \dot{\tilde{d}}_1 &= -l_3 \text{sig}^{m_3}(\tilde{\eta}) \end{aligned} \tag{16}$$

Define the system matrix  $\mathbf{A} = \begin{pmatrix} -l_1 I_3 & I_3 & 0 \\ -l_2 I_3 & 0 & I_3 \\ -l_3 I_3 & 0 & 0 \end{pmatrix}$  and  $\mathbf{A}$  as the Hurwitz matrix. Then, the Lyapunov function is written as follows:

$$V_m(\tilde{\omega}_1, \tilde{\omega}_2, \tilde{\omega}_3) = \omega^T \mathbf{P} \omega \tag{17}$$

where  $\omega = [\tilde{\omega}_1^T, \tilde{\omega}_2^T, \tilde{\omega}_3^T]^T = [[\text{sig}^{\frac{1}{\sigma}}(\tilde{\eta})]^T, [\text{sig}^{\frac{1}{\sigma m_1}}(\tilde{\mu})]^T, [\text{sig}^{\frac{1}{\sigma m_2}}(\tilde{d})]^T]^T$ ,  $\sigma = m_1 m_2 m_3$ , and  $\mathbf{P}$  is positive with respect to  $\mathbf{A}^T \mathbf{P} + \mathbf{P} \mathbf{A} = -\mathbf{I}_9$ . By [29], define  $f_m$  as the vector field and set  $L_{f_m} V_m(\tilde{\omega}_1, \tilde{\omega}_2, \tilde{\omega}_3)$  as the Lie derivative of  $V_m(\tilde{\omega}_1, \tilde{\omega}_2, \tilde{\omega}_3)$  along the vector field  $f_m$ . According to Definition 1,  $V_m(\tilde{\omega}_1, \tilde{\omega}_2, \tilde{\omega}_3)$  and  $L_{f_m} V_m(\tilde{\omega}_1, \tilde{\omega}_2, \tilde{\omega}_3)$  can be obtained such that they are homogeneous with degrees  $\frac{2}{\sigma}$  and  $\frac{2}{\sigma} + m_1 - 1$  with respect to  $(1, m_1, 2m_1 - 1)$ , respectively, and the inequality  $L_{f_m} V_m(\tilde{\omega}_1, \tilde{\omega}_2, \tilde{\omega}_3) \leq -c_1 [V_m(\tilde{\omega}_1, \tilde{\omega}_2, \tilde{\omega}_3)]^\varepsilon$  is established, where  $c_1 = -\max_{\{x_i: V_m(x)=1\}} L_{f_m} V_m$  and  $\varepsilon = 1 + \frac{m_1 \sigma}{2} - \frac{\sigma}{2} < 1$ . Choose the Lyapunov function candidate of the error subsystem (8) as follows:

$$V_{of}(\tilde{\omega}_1, \tilde{\omega}_2, \tilde{\omega}_3) = \omega^T \mathbf{P} \omega \tag{18}$$

Taking the time derivative of (18) alongside (15), we can obtain

$$\begin{aligned} \dot{V}_{of} &= L_{f_m} V_m(\tilde{\omega}_1, \tilde{\omega}_2, \tilde{\omega}_3) + 2\omega^T \mathbf{P} \begin{bmatrix} -diag(|\tilde{\eta}|^{\frac{1}{\sigma}}) \lambda_1 \text{sgn}(\tilde{\eta}) \\ -diag(|\tilde{\mu}|^{\frac{1}{\sigma m_1}}) \lambda_2 \text{sgn}(\tilde{\eta}) \\ -diag(|\tilde{d}|^{\frac{1}{\sigma m_2}-1}) (-\dot{d} - \lambda_3 \text{sgn}(\tilde{\eta})) \end{bmatrix} \\ &\leq -c_1 V_{of} + \frac{2\lambda_1 \lambda_{\max}(\mathbf{P}) \|\omega\| \sum_{i=1}^3 |\tilde{\eta}_i|^{\frac{1}{\sigma}-1}}{\sigma} \\ &\quad + \frac{2\lambda_2 \lambda_{\max}(\mathbf{P}) \|\omega\| \sum_{i=1}^3 |\tilde{\mu}_i|^{\frac{1}{\sigma m_1}-1}}{\sigma m_1} \\ &\quad + \frac{2(d_m + \lambda_3) \lambda_{\max}(\mathbf{P}) \|\omega\| \sum_{i=1}^3 |\tilde{d}_i|^{\frac{1}{\sigma m_2}-1}}{\sigma m_2} \end{aligned} \tag{19}$$

On the basis of Lemma 2, it yields

$$\sum_{i=1}^3 |\tilde{\eta}_i|^{\frac{1}{\sigma}-1} \leq 3^\sigma \left( \sum_{i=1}^3 |\tilde{\eta}_i|^{\frac{1}{\sigma}} \right)^{1-\sigma} \leq 3^{\frac{1+\sigma}{2}} \|\omega\|^{1-\sigma} \tag{20}$$

$$\sum_{i=1}^3 |\tilde{\mu}_i|^{\frac{1}{\sigma m_1}-1} \leq 3^{\sigma m_1} \left( \sum_{i=1}^3 |\tilde{\mu}_i|^{\frac{1}{\sigma m_1}} \right)^{1-\sigma m_1} \leq 3^{\frac{1+\sigma m_1}{2}} \|\omega\|^{1-\sigma m_1} \tag{21}$$

$$\sum_{i=1}^3 |\tilde{d}_i|^{\frac{1}{\sigma m_2}-1} \leq 3^{\sigma m_2} \left( \sum_{i=1}^3 |\tilde{d}_i|^{\frac{1}{\sigma m_2}} \right)^{1-\sigma m_2} \leq 3^{\frac{1+\sigma m_2}{2}} \|\omega\|^{1-\sigma m_2} \tag{22}$$

Substituting (20)–(22) into (19) yields

$$\begin{aligned} \dot{V}_{of} &\leq -c_1 V_{of}^\varepsilon + \frac{2 \times 3^{\frac{1+\sigma}{2}} \lambda_1 \lambda_{\max}(\mathbf{P}) \|\omega\|^{2-\sigma}}{\sigma} \\ &\quad + \frac{2 \times 3^{\frac{1+\sigma m_1}{2}} \lambda_2 \lambda_{\max}(\mathbf{P}) \|\omega\|^{2-\sigma m_1}}{\sigma m_1} \\ &\quad + \frac{2 \times 3^{\frac{1+\sigma m_2}{2}} (d_m + \lambda_3) \lambda_{\max}(\mathbf{P}) \|\omega\|^{2-\sigma m_2}}{\sigma m_2} \\ &\leq -c_1 V_{of}^\varepsilon + c_2 V_{of}^{1-\frac{\sigma}{2}} + c_3 V_{of}^{1-\frac{\sigma m_1}{2}} + c_4 V_{of}^{1-\frac{\sigma m_2}{2}} \end{aligned} \tag{23}$$

where

$$c_2 = \frac{2 \times 3^{\frac{1+\sigma}{2}} \lambda_1 \lambda_{\max}(\mathbf{P})}{\sigma [\lambda_{\min}(\mathbf{P})]^{1-\frac{\sigma}{2}}} \tag{24}$$

$$c_3 = \frac{2 \times 3^{\frac{1+\sigma m_1}{2}} \lambda_2 \lambda_{\max}(\mathbf{P})}{\sigma m_1 [\lambda_{\min}(\mathbf{P})]^{\frac{1-\sigma m_1}{2}}}, \quad c_4 = \frac{2 \times 3^{\frac{1+\sigma m_2}{2}} (d_m + \lambda_3) \lambda_{\max}(\mathbf{P})}{\sigma m_2 [\lambda_{\min}(\mathbf{P})]^{\frac{1-\sigma m_2}{2}}}$$

Since  $0 < 1 - \frac{\sigma}{2} < 1 - \frac{\sigma m_1}{2} < 1 - \frac{\sigma m_2}{2} < \varepsilon < 1$ , the following two situations are taken into account for further research.

If  $V_{of} \geq 1$ , we can simplify (24) as follows:

$$\dot{V}_{of} \leq -c_1 V_{of}^\varepsilon + c_0 V_{of} \tag{25}$$

where  $c_0 = c_2 + c_3 + c_4$ . With respect to Lemma 1, it can be deduced that  $t_{01}$  and  $V_{of}$  converge to  $V_{of} = 1$ , i.e.,  $t_{01} \leq \ln \frac{1 - \frac{c_0}{c_1} V_{of}^{1-\varepsilon}(0)}{c_0 \varepsilon - c_0}$ .

If  $V_{of} \leq 1$ , we can simplify (24) as

$$\begin{aligned} \dot{V}_{of} &\leq -c_1 V_{of}^\epsilon + c_0 V_{of}^{1-\frac{\sigma}{2}} \\ &\leq -c_1 \bar{c}_0 V_{of}^\epsilon - [c_1(1-\bar{c}_0)V_{of}^{\epsilon-1+\frac{\sigma}{2}} - c_0]V_{of}^{1-\frac{\sigma}{2}} \end{aligned} \tag{26}$$

where  $0 < \bar{c}_0 < 1 - \frac{c_0}{c_1}$ ; hence, when  $V_{of}^{\epsilon-1+\frac{\sigma}{2}} > \frac{c_0}{c_1(1-\bar{c}_0)}$ ,  $\dot{V}_{of} \leq -c_1 \bar{c}_0 V_{of}^\epsilon$  and  $V_{of}$  is decreasing. Based on Lemma 1, the convergence time  $t_{o2} \leq \ln \frac{V_{of}^{1-\epsilon}(\omega(t_{o1}))}{c_1 \bar{c}_0 (1-\epsilon)}$  such that  $V_{of}$  converges to the domain.

$$V_{of} > \left(\frac{c_0}{c_1(1-\bar{c}_0)}\right)^{\frac{2}{\sigma m_1}} \tag{27}$$

Next, it can be seen that the Lyapunov function  $V_{of}$  converges to region (27) within the time  $T_1 = t_{o1} + t_{o2} < \infty$ .

Substituting (18) into (27), the observation error  $\omega$  can be obtained as below:

$$\|\omega\| < \frac{1}{\sqrt{\lambda_{\min}(\mathbf{P})}} \left(\frac{c_0}{c_1(1-\bar{c}_0)}\right)^{\frac{1}{\sigma m_1}} \tag{28}$$

According to Lemma 3, it can be obtained that

$$\|\tilde{\eta}\| \leq \sum_{i=1}^3 (|\tilde{\eta}_i|^{\frac{1}{\sigma}})^\sigma \leq 3^{1-\sigma} \left(\sum_{i=1}^3 |\tilde{\eta}_i|^{\frac{1}{\sigma}}\right)^\sigma \leq 3^{1-\frac{\sigma}{2}} \|\omega\|^\sigma \tag{29}$$

$$\|\tilde{\mu}_i\| \leq \sum_{i=1}^3 (|\tilde{\mu}_i|^{\frac{1}{\sigma m_1}})^{\sigma m_1} \leq 3^{1-\sigma m_1} \left(\sum_{i=1}^3 |\tilde{\mu}_i|^{\frac{1}{\sigma m_1}}\right)^{\sigma m_1} \leq 3^{1-\frac{\sigma m_1}{2}} \|\omega\|^{\sigma m_1} \tag{30}$$

$$\|\tilde{d}_i\| \leq \sum_{i=1}^3 (|\tilde{d}_i|^{\frac{1}{\sigma m_2}})^{\sigma m_2} \leq 3^{1-\sigma m_2} \left(\sum_{i=1}^3 |\tilde{d}_i|^{\frac{1}{\sigma m_2}}\right)^{\sigma m_2} \leq 3^{1-\frac{\sigma m_2}{2}} \|\omega\|^{\sigma m_2} \tag{31}$$

Substituting (28) into (29)–(31), the convergence of the estimation error can be rewritten as follows:

$$\|\tilde{\eta}\| \leq \frac{3^{1-\frac{\sigma}{2}}}{\sqrt{\lambda_{\min}(\mathbf{P})}^\sigma} \left(\frac{c_0}{c_1(1-\bar{c}_0)}\right)^{\frac{1}{m_1}} \tag{32}$$

$$\|\tilde{\mu}\| \leq \frac{3^{1-\frac{\sigma m_1}{2}}}{\sqrt{\lambda_{\min}(\mathbf{P})}^{\sigma m_1}} \left(\frac{c_0}{c_1(1-\bar{c}_0)}\right) \tag{33}$$

$$\|\tilde{d}_1\| \leq \frac{3^{1-\frac{\sigma m_2}{2}}}{\sqrt{\lambda_{\min}(\mathbf{P})}^{\sigma m_2}} \left(\frac{c_0}{c_1(1-\bar{c}_0)}\right)^{\frac{m_2}{m_1}} \tag{34}$$

Obviously, the errors  $\tilde{\eta}$ ,  $\tilde{\mu}$ , and  $\tilde{d}$  can converge to a bounded domain within finite time; then, set  $\lambda_i (i = 1, 2, 3)$  properly and the errors can also converge to equilibrium.

Choose a Lyapunov candidate for  $\tilde{\eta}$

$$V_{o1} = \frac{1}{2} \tilde{\eta}^T \tilde{\eta} \tag{35}$$

Take the derivative of  $V_{o1}$  as follows:

$$\begin{aligned} \dot{V}_{o1} &= \tilde{\eta}^T \dot{\tilde{\eta}} = \tilde{\eta}^T [\tilde{\mu} - l_1 \text{sig}^{m_1}(\tilde{\eta}) - \lambda_1 \text{sgn}(\tilde{\eta})] \\ &\leq \|\tilde{\eta}\| \|\tilde{\mu}\| - l_1 \sum_{i=1}^3 |\tilde{\eta}|^{m_1+1} - \lambda_1 \sum_{i=1}^3 |\tilde{\eta}| \\ &\leq -(\lambda_1 - \|\tilde{\mu}\|) \|\tilde{\eta}\| - \frac{l_1}{3^{\frac{m_1}{2}}} \|\tilde{\eta}\|^{m_1+1} \end{aligned} \tag{36}$$

since  $\|\tilde{\mu}\| \leq \frac{3^{1-\frac{\sigma m_1}{2}}}{\sqrt{\lambda_{\min}(\mathbf{P})}^{\sigma m_1}} (\frac{c_0}{c_1(1-\bar{c}_0)})$ ,  $c_0 = c_2 + c_3 + c_4$ , and  $c_2 = \frac{2 \times 3^{\frac{1+\sigma}{2}} \lambda_1 \lambda_{\max}(\mathbf{P})}{\sigma[\lambda_{\min}(\mathbf{P})]^{\frac{1-\sigma}{2}}}$ , choose  $\lambda_1 \geq \|\tilde{\mu}\|$ , i.e.,  $\lambda_1 \geq \frac{3^{1-\frac{\sigma m_1}{2}} \sigma[\lambda_{\min}(\mathbf{P})]^{1-\frac{\sigma}{2}} (c_3+c_4)}{[\sigma[\lambda_{\min}(\mathbf{P})]^\epsilon (1-\bar{c}_0) - 2 \times 3^{\frac{3+\sigma-\sigma m_1}{2}} \lambda_{\max}(\mathbf{P})]}$ . It can be demonstrated that the control design parameter  $\lambda_1$  is independent. Next, formula (36) becomes  $\dot{V}_{o1} \leq -c_{o1} V_{o1}^{\frac{m_1+1}{2}}$ , where  $c_{o1} = \frac{2}{3^{\frac{m_1+1}{2}}} l_1$ . Thus, the error  $\tilde{\eta}$  can converge to 0 within finite time  $t_{o3} \leq \frac{2V_{of}^{\frac{1-m_1}{2}} (\tilde{\eta}(T_1))}{c_{o1}(1-m_1)}$ . After the time  $T_2 = T_1 + t_{o3}$ , the second subsystem (15) is written as follows:

$$\dot{\tilde{\mu}} = \tilde{d}_1 - \lambda_2 \text{sgn}(\tilde{\mu}) \tag{37}$$

Accordingly, select the Lyapunov function for  $\tilde{\mu}$  as follows:

$$V_{o2} = \frac{1}{2} \tilde{\mu}^T \tilde{\mu} \tag{38}$$

The derivative of (38) is

$$\begin{aligned} \dot{V}_{o2} &\leq \tilde{\mu}^T \dot{\tilde{\mu}} = \tilde{\mu}^T [\tilde{d}_1 - \lambda_2 \text{sgn}(\tilde{\mu})] \\ &\leq -(\lambda_2 - \|\tilde{d}_1\|) \|\tilde{\mu}\| \end{aligned} \tag{39}$$

By choosing the appropriate parameter  $\lambda_2$ ,  $\lambda_2 \geq \|\tilde{d}_1\| + \epsilon_1$  holds. As  $\|\tilde{d}_1\| \leq \frac{3^{1-\frac{\sigma m_2}{2}}}{\sqrt{\lambda_{\min}(\mathbf{P})}^{\sigma m_2}} (\frac{c_0}{c_1(1-\bar{c}_0)})^{\frac{m_2}{m_1}}$  and  $c_3 = \frac{2 \times 3^{\frac{1+\sigma m_1}{2}} \lambda_2 \lambda_{\max}(\mathbf{P})}{\sigma m_1 [\lambda_{\min}(\mathbf{P})]^{\frac{1-\sigma m_1}{2}}}$ , the control parameter  $\lambda_2$  is similarly independent from the system. Based on Lemma 1,  $\tilde{\mu}$  could converge to zero within  $t_{o4} \leq \frac{\sqrt{2}}{\epsilon_1} V_{o2}(\tilde{\mu})^{\frac{1}{2}}_{T_2}$ .

After the time  $T_3 = T_2 + t_{o4}$ , the third equation of (15) is written as follows:

$$\dot{\tilde{d}}_1 = -\tilde{d}_1 - \lambda_3 \text{sgn}(\tilde{d}_1) \tag{40}$$

In the same way, choose the Lyapunov candidate for  $\tilde{d}_1$  as

$$V_{o3} = \frac{1}{2} \tilde{d}_1^T \tilde{d}_1 \tag{41}$$

The derivative of (41) is

$$\begin{aligned} \dot{V}_{o3} &\leq \tilde{d}_1^T \dot{\tilde{d}}_1 = \tilde{d}_1^T [-\tilde{d}_1 - \lambda_3 \text{sgn}(\tilde{d}_1)] \\ &\leq -(\lambda_3 + \|\dot{\tilde{d}}_1\|) \|\tilde{d}_1\| \end{aligned} \tag{42}$$

By choosing the appropriate parameter,  $\lambda_3$ ,  $\lambda_3 + \|\dot{\tilde{d}}_1\| \geq \epsilon_2$  are fulfilled. When  $\|\dot{\tilde{d}}_1\| \leq d_m$ , the control parameter  $\lambda_3$  is independent from the system. As such, with the above parameter selection,  $\tilde{d}_1$  could converge to zero within  $t_{o5} \leq \frac{\sqrt{2}}{\epsilon_2} V_{o3}(\tilde{d}_1)^{\frac{1}{2}}_{T_3}$ .

Based on the aforementioned sections, the estimation errors  $\tilde{\eta}$ ,  $\tilde{\mu}$ , and  $\tilde{d}_1$  could converge to zero within the finite time  $T_4 = T_3 + t_{o5}$ .

The proof is completed.  $\square$

**Remark 4.** With the FTESO, note that a hovercraft's states are assumed to be bounded; next, the estimation errors will converge to the residual set  $\Omega_1$ :

$$\Omega_1 = \left\{ \begin{aligned} & (\omega_1, \omega_2, \omega_3) \mid \|(\omega_1, \omega_2, \omega_3)\| \leq \frac{3^{1-\frac{\sigma}{2}}}{\sqrt{\lambda_{\min}(\mathbf{P})}^\sigma} \left(\frac{c_4}{(c_1(1-c_0)-c_3)}\right)^{\frac{1}{m_3}} \\ & + \frac{3^{1-\frac{\sigma m_2}{2}}}{\sqrt{\lambda_{\min}(\mathbf{P})}^{\sigma m_1}} \left(\frac{c_4}{(c_1(1-c_0)-c_3)}\right)^{\frac{m_1}{m_3}} + \frac{3^{1-\frac{\sigma m_2}{2}}}{\sqrt{\lambda_{\min}(\mathbf{P})}^{\sigma m_2}} \left(\frac{c_4}{(c_1(1-c_0)-c_3)}\right)^{\frac{m_2}{m_3}} \end{aligned} \right\}. \text{ The residual set's}$$

$\Omega_1$  size relies on the minimum eigenvalue of  $\mathbf{P}$ . It is noted that the residual set  $\Omega_1$  can be as small as desired by designing  $\mathbf{P}$ .

### 3.2. Design of LOS

In this subsection, in the presence of time-varying sideslip compensation, an adaptive BGF-LOS guidance law is developed to obtain better performance for a hovercraft subjected to sideslip constraint during path following.

First of all, for the sake of estimating the sideslip angle parameter varying with time, the model is represented as a vector form. We firstly define

$$x = [x_e \ y_e]^T, \theta(t) = \tan \beta(t), \mathbf{h}(x) = [u \cos(\psi - \psi_F(\vartheta)) + \dot{\psi}_F(\vartheta)y_e - \dot{\vartheta} \sqrt{x_F^2(\vartheta) + y_F^2(\vartheta)} \ u \sin(\psi - \psi_F(\vartheta)) - \dot{\psi}_F(\vartheta)x_e]^T, \text{ and } \tilde{\lambda}(x) = [-u \sin(\psi - \psi_F(\vartheta)) \ u \cos(\psi - \psi_F(\vartheta))]^T; \text{ next, the error dynamics (9) are constructed as}$$

$$\dot{x} = \mathbf{h}(x) + \tilde{\lambda}(x)\theta(t) \tag{43}$$

Next, we define the state predictor model for (43) as below [30]:

$$\dot{\hat{x}} = \mathbf{h}(x) + \tilde{\lambda}(x)\hat{\theta}(t) + \mathbf{k}_{sw}e_{xs} + w\dot{\hat{\theta}}(t), \mathbf{k}_{sw} > 0 \tag{44}$$

$$\dot{w} = -\mathbf{k}_{sw}w + \tilde{\lambda}(x), w(t_0) = 0 \tag{45}$$

where  $\hat{x} = [\hat{x}_e \ \hat{y}_e]^T$  is the predicted vector of  $x = [x_e \ y_e]^T$ ;  $e_{xs} = x - \hat{x}$  is the estimation error;  $\mathbf{k}_{sw} \in \mathbf{R}^{2 \times 2}$  with respect to  $\mathbf{k}_{sw} + \mathbf{k}_{sw}^T \succ \mathbf{I}$ ;  $w \in \mathbf{R}^{2 \times 1}$  is the output of (44); and  $\hat{\theta}(t)$  is the estimation of sideslip parameter, which is generated by the update law  $\dot{\hat{\theta}}(t)$  proposed below.

Noting that the sideslip angle estimation error  $\tilde{\theta} = \theta - \hat{\theta}$ , it is obtained in (43) and (44) that

$$\dot{e}_{xs} = \tilde{\lambda}(x)\tilde{\theta}(t) - \mathbf{k}_{sw}e_{xs} - w\dot{\hat{\theta}}(t) \tag{46}$$

Next,  $\zeta$  is an auxiliary variable, which is defined as  $\zeta = e_{xs} - w\tilde{\theta}(t)$ ; it is obtained from (45) and (46) that

$$\dot{\zeta} = -\mathbf{k}_{sw}\zeta - w\dot{\hat{\theta}}(t), \zeta(t_0) = e_{xs}(t_0) \tag{47}$$

Because the change rate of the sideslip parameter  $\dot{\theta}(t)$  is unavailable, we can obtain an estimation of  $\zeta$  [31] as follows:

$$\dot{\hat{\zeta}} = -\mathbf{k}_{sw}\hat{\zeta} \tag{48}$$

Define the estimation error  $\tilde{\zeta} = \zeta - \hat{\zeta}$  with dynamics

$$\dot{\tilde{\zeta}} = -\mathbf{k}_{sw}\tilde{\zeta} - w\dot{\hat{\theta}}(t), \tilde{\zeta}(t_0) = 0 \tag{49}$$

based on the definitions of  $\zeta$  and  $\tilde{\zeta}$ , we have

$$w\tilde{\theta}(t) = e_{xs} - \tilde{\zeta} - \hat{\zeta} \tag{50}$$

Based on (44), (45), and (48), consider the BGF estimator as [32]

$$\dot{\hat{\theta}} = \text{Proj}\{\Xi^{-1}(w^T(e_{xs} - \hat{\zeta}) - \tilde{\lambda}\hat{\theta}), \hat{\theta}\}, \hat{\theta}(t_0) = \theta^0 \tag{51}$$

where the gain  $\Xi \in \mathbb{R}^{n\theta \times n\theta}$  can be obtained from the following update law:

$$\begin{cases} \dot{\Xi}^{-1} = -\Xi^{-1}w^T w \Xi^{-1} + \lambda_T \Xi^{-1} - \delta_s \Xi^{-1} \Xi^{-1}; \Xi^{-1}(t_0) = \alpha_s^{-1} \\ \dot{\Xi} = -\lambda_T(\Xi - \delta_s / \lambda_T) + w^T w; \Xi(t_0) = \alpha_s \end{cases} \tag{52}$$

where  $\lambda_T$  is a design positive factor;  $\delta_s$  is a design control parameter; and  $\text{Proj}\{\phi, \hat{\theta}\}$  represents the Lipschitz projection operator, which meets with [33]

$$-\text{Proj}\{\phi, \hat{\theta}(t)\}^T \tilde{\theta}(t) \leq -\phi^T \tilde{\theta}(t) \tag{53}$$

Then, we select the path-following laws as follows:

$$\begin{cases} \psi_d = \psi_F(\vartheta) + a \tan\left(-\frac{y_e + \alpha_y}{\Delta}\right) \\ \dot{\vartheta} = \frac{u_d \cos(\psi - \psi_F(\vartheta)) + u_d \sin(\psi - \psi_F(\vartheta)) \hat{\theta} + k_{s1} x_e}{\sqrt{x_F^2(\vartheta) + y_F^2(\vartheta)}} \\ \alpha_r = -k_\psi(\psi - \psi_d) - k_{\psi_1} \text{sig}^{1/2}(\psi - \psi_d) + \dot{\psi}_d - y_e \sqrt{\hat{u}^2 + \hat{v}^2} \varphi \end{cases} \tag{54}$$

where  $\varphi = \frac{(1 - \cos \tilde{\psi})(y_e + \alpha_y) + \Delta \sin \tilde{\psi}}{\tilde{\psi} \sqrt{(y_e + \alpha_y)^2 + \Delta^2}}$ ,  $\alpha_y = \text{sig}^{1/2}(y_e)$ , and

$$\begin{aligned} 0 < \Delta_{\min} < \Delta \leq \Delta_{\max} \left| \frac{\Delta}{\sqrt{(y_e + \alpha_y)^2 + \Delta^2}} \right| &\leq 1 \left| \frac{y_e + \alpha_y}{\sqrt{(y_e + \alpha_y)^2 + \Delta^2}} \right| \\ &\leq 1 \left| \frac{\sin(\psi - \psi_d)}{\psi - \psi_d} \right| \leq 1 \left| \frac{1 - \cos(\psi - \psi_d)}{\psi - \psi_d} \right| < 0.73 \end{aligned}$$

so,  $|\varphi| < 1.73$  is bounded.

Therefore, the error dynamics  $x_e$  and  $y_e$  can be established as

$$\begin{cases} \dot{x}_e = -k_{s1} x_e + u \sin(\psi - \psi_F(\vartheta)) \tilde{\theta} + \dot{\psi}_F(\vartheta) y_e \\ \dot{y}_e = \frac{-u y_e}{\sqrt{x_F^2(\vartheta) + y_F^2(\vartheta)}} + u \cos(\psi - \psi_F(\vartheta)) \tilde{\theta} - \dot{\psi}_F(\vartheta) y_e \end{cases} \tag{55}$$

We choose the Lyapunov function  $V_E = \frac{1}{2} x_e^2 + \frac{1}{2} y_e^2$  regarding position errors. Then, we can obtain

$$\dot{V}_E = -k_{s1} x_e^2 + u \sin(\psi - \psi_F(\vartheta)) x_e \tilde{\theta} - k_{sc} y_e^2 + u \cos(\psi - \psi_F(\vartheta)) y_e \tilde{\theta} \tag{56}$$

where  $k_{sc} = \frac{u}{\sqrt{(y_e + \Delta \hat{\theta})^2 + \Delta^2}} > 0$ .

By Young's inequality,

$$\begin{cases} u \sin(\psi - \psi_F(\vartheta)) x_e \tilde{\theta} \leq \frac{u}{2\epsilon_{s1}} |x_e|^2 + \frac{u\epsilon_{s1}}{2} |\tilde{\theta}|^2 \\ u \cos(\psi - \psi_F(\vartheta)) y_e \tilde{\theta} \leq \frac{u}{2\epsilon_{s2}} |y_e|^2 + \frac{u\epsilon_{s2}}{2} |\tilde{\theta}|^2 \end{cases} \tag{57}$$

It follows that

$$\begin{aligned} \dot{V}_E &\leq -(k_{s1} - u/(2\epsilon_{s1})) x_e^2 - (k_{sc} - u/(2\epsilon_{s2})) y_e^2 + \frac{u}{2} (\epsilon_{s1} + \epsilon_{s2}) |\tilde{\theta}|^2 \\ &\leq -2k_{s\min} V_E + \frac{u}{2} (\epsilon_{s1} + \epsilon_{s2}) |\tilde{\theta}|^2 \end{aligned} \tag{58}$$

where  $k_{s\min} = \min\{k_{s1} - u/(2\epsilon_{s1}), (k_{sc} - u/(2\epsilon_{s2}))\} > 0$ .

Noting that  $E = [x_e, y_e]^T$ , one has

$$\dot{V}_E \leq -\frac{1}{2} k_{s\min} \|E\|^2 - \left(\frac{1}{2} k_{s\min} \|E\|^2 - \frac{u}{2} (\epsilon_{s1} + \epsilon_{s2}) |\tilde{\theta}|^2\right) \tag{59}$$

and since [34]

$$\|E\| \geq \frac{\sqrt{u\epsilon_{s1}} |\tilde{\theta}|}{\sqrt{k_{s\min}}} + \frac{\sqrt{u\epsilon_{s2}} |\tilde{\theta}|}{\sqrt{k_{s\min}}} \geq \sqrt{\frac{u(\epsilon_{s1} + \epsilon_{s2}) |\tilde{\theta}|^2}{k_{s\min}}} \tag{60}$$

this renders

$$\dot{V}_E \leq -\frac{1}{2}k_{s\min}\|E\|^2 \tag{61}$$

Choosing  $\alpha_{01}(\|E\|) = \alpha_{02}(\|E\|) = \|E\|^2/2 = V_E$ , there is a class  $\mathcal{KL}$  function  $\delta_{\mathcal{KL}2}(E(t_0), t) = e^{-k_{s\min}t/2}E(t_0)$  and a class  $\mathcal{K}$  function  $\rho_{s2}(x) = \sqrt{u(\varepsilon_{s1} + \varepsilon_{s2})/2}x$  such that  $\gamma_{01} = \alpha_{01}^{-1} \circ \alpha_{02} \circ \rho_{s2} = \rho_{s2}$  and  $\|E(t)\| \leq \delta_{\mathcal{KL}2}(E(t_0), t) + \rho_{s2}(|\theta|)$ .

Consequently, Equation (61) is referenced to study the whole system’s stability.

### 3.3. Safety-Guaranteed, Robust, Nonlinear, Path-Following Controller

#### 3.3.1. Safety-Guaranteed Auxiliary System Subject to Constraints

The safety auxiliary system’s input of drift angle  $\beta$  is defined as follows:

$$\Delta\beta = k_\beta(\beta_{\max} - \beta) \tag{62}$$

where  $k_\beta$  is a positive constant and  $\beta_{\max}$  can be designed as follows:

$$\beta_{\max} = \text{sat}(\beta, \beta_{\max}, \beta_{\min}) = \begin{cases} \beta_{\max} & \beta > \beta_{\max} \\ \beta & \beta_{\min} \leq \beta \leq \beta_{\max} \\ \beta_{\min} & \beta < \beta_{\min} \end{cases} \tag{63}$$

Devise the safety auxiliary system with the following constraint [35]:

$$\dot{\zeta}_\beta = \begin{cases} -k_{\zeta\beta_1}\zeta_\beta - k_{\zeta\beta_2}\text{sig}^{\frac{1}{2}}(\zeta_\beta) \\ -\frac{\frac{1}{2}(k_{\zeta\beta_3}\Delta\beta)^2}{|\zeta_\beta|^2}\zeta_\beta + k_{\zeta\beta_3}\Delta\beta, & |\zeta_\beta| \geq \delta \\ 0, & |\zeta_\beta| < \delta \end{cases} \tag{64}$$

where  $k_{\zeta\beta_1} > 1$ ,  $k_{\zeta\beta_2} > 0$ , and  $k_{\zeta\beta_3} > 0$  are parameters of the safety-guaranteed auxiliary system designed later on and  $\delta > 0$  is a very small constant.

#### 3.3.2. FTESO-Based Safety-Guaranteed Heading-Tracking Control Strategy

Let  $\mu = S(\psi)v$  and  $v = S^T(\psi)\mu$ ; thus,  $\hat{V} = S^T(\hat{\psi})\hat{\mu}$ . The path-following error of the yaw angle is denoted below:

$$\hat{r}_e = \hat{r} - \alpha_r \tag{65}$$

where  $\alpha_r$  is the virtual control law.

Differentiating (65) and reconstructing (14), we can obtain

$$\dot{\hat{r}}_e = \hat{r}\hat{\mu}_r - l_2\text{sig}^{m_2}(\tilde{\psi}) + \hat{d}_r + J_z^{-1}\tau_r - \lambda_2\text{sig}^{m_2}(\tilde{\psi}) - \dot{\alpha}_r \tag{66}$$

For the sake of stabilizing the yaw angle error (66), the FTESO-based, robust, nonlinear heading-tracking controller is introduced as follows:

$$\begin{aligned} \tau_r &= \tau_{rc} + \tau_{r\beta} = J_z(-k_r\hat{r}_e - k_{r_1}\text{sig}^{\frac{1}{2}}(\hat{r}_e) - \hat{r}\hat{\mu}_r \\ &+ l_2\text{sig}^{m_2}(\tilde{\psi}) + \lambda_2\text{sig}^{m_2}(\tilde{\psi}) - \hat{d}_r + \dot{\alpha}_r) \\ &+ \frac{1}{2}(k_{\zeta\beta_3}\Delta\hat{\beta})^2 - k_{\zeta\beta_3}\Delta\hat{\beta}\hat{\zeta}_\beta \end{aligned} \tag{67}$$

where  $k_r > 0$ ,  $k_{r_1} > 0$ , and  $k_{\zeta\beta_3} > 0$  are the design parameters.

Substituting the controller (67) into (66), we can obtain

$$\dot{\hat{r}}_e = -k_r\hat{r}_e - k_{r_1}\text{sig}^{\frac{1}{2}}(\hat{r}_e) - \psi_e \tag{68}$$

#### 3.3.3. FTESO-Based Safety-Guaranteed, Robust, Nonlinear, Tracking Control Design

According to the velocity observation, the velocity tracking error of the hovercraft is denoted as follows:

$$\hat{u}_e = \hat{u} - u_d \tag{69}$$

Differentiating (62) and rewriting (14), we obtain

$$\begin{aligned} \hat{u}_e &= \cos(\hat{\psi})(-l_2 \text{sig}^{m_2}(\tilde{x}) + \tilde{d}_u + \cos(\psi)m^{-1}\tau_u - \lambda_2 \text{sgn}(\tilde{x})) \\ &+ \sin(\hat{\psi})(-l_2 \text{sig}^{m_2}(\tilde{y}) + \tilde{d}_v + \sin(\psi)m^{-1}\tau_u - \lambda_2 \text{sgn}(\tilde{y})) \\ &- \dot{u}_d - \hat{r} \sin(\hat{\psi})\hat{\rho}_u + \hat{r} \cos(\hat{\psi})\hat{\rho}_v \\ &= m^{-1}\tau_u(\cos(\hat{\psi}) \cos(\psi) + \sin(\hat{\psi}) \sin(\psi)) - \hat{r} \sin(\hat{\psi})\hat{\rho}_u \\ &+ \cos(\hat{\psi})(-l_2 \text{sig}^{m_2}(\tilde{x}) + \tilde{d}_u - \lambda_2 \text{sgn}(\tilde{x})) + \hat{r} \cos(\hat{\psi})\hat{\rho}_u \\ &\sin(\hat{\psi})(-l_2 \text{sig}^{m_2}(\tilde{y}) + \tilde{d}_v - \lambda_2 \text{sgn}(\tilde{y})) - \dot{u}_d \end{aligned} \tag{70}$$

For the sake of stabilizing the surge velocity error formula (70), the robust, nonlinear, velocity-tracking controller is introduced as follows:

$$\begin{aligned} \tau_u &= H^{-1}m(-k_u \hat{u}_e - k_{u_1} \text{sig}^{\frac{1}{2}}(\hat{u}_e) + \hat{r} \sin(\hat{\psi})\hat{\rho}_u - \hat{r} \cos(\hat{\psi})\hat{\rho}_v) \\ &- \cos(\hat{\psi})(-l_2 \text{sig}^{m_2}(\tilde{x}) + \tilde{d}_u - \lambda_2 \text{sgn}(\tilde{x})) \\ &- \sin(\hat{\psi})(-l_2 \text{sig}^{m_2}(\tilde{y}) + \tilde{d}_v - \lambda_2 \text{sgn}(\tilde{y})) + \dot{u}_d \end{aligned} \tag{71}$$

where

$$H = \cos(\hat{\psi}) \cos(\psi) + \sin(\hat{\psi}) \sin(\psi) \tag{72}$$

Combining (71) with (70), it can be obtained that

$$u_e = -k_u \hat{u}_e - k_{u_1} \text{sig}^{\frac{1}{2}}(\hat{u}_e) \tag{73}$$

Choose the Lyapunov function for the control subsystem as below,

$$V_c = \frac{1}{2} \hat{u}_e^2 + \frac{1}{2} \hat{r}_e^2 + \frac{1}{2} \hat{\zeta}_\beta^2 \tag{74}$$

and taking the time derivative of  $V_c$ , we obtain

$$\begin{aligned} \dot{V}_c &= \hat{u}_e \dot{\hat{u}}_e + \hat{r}_e \dot{\hat{r}}_e + \hat{\zeta}_\beta \dot{\hat{\zeta}}_\beta \\ &\leq -k_u \hat{u}_e^2 - k_{u_1} |\hat{u}_e|^{\frac{3}{2}} - k_r \hat{r}_e^2 - k_{r_1} |\hat{r}_e|^{\frac{3}{2}} - k_{\zeta\beta_1} \hat{\zeta}_\beta^2 - k_{\zeta\beta_2} |\hat{\zeta}_\beta|^{\frac{3}{2}} \end{aligned} \tag{75}$$

Equation (75) is used to solve the system stability.

#### 4. Stability Analysis

**Theorem 2.** For a hovercraft depicted in (12) with regard to the unknown model dynamics and external ocean disturbances, taking Assumptions 1-6 into consideration, combine the FTESO (14); BGF-LOS guidance laws (54) and (55); and the safety-guaranteed, robust, nonlinear controllers (67) and (71). Then, the path-following errors could converge to the origin with the performance guarantee required on all states being uniformly, ultimately bounded at the same time in the closed-loop control system via selecting the control coefficients appropriately.

**The Proof of Theorem 2.** Select the candidate as follows:

$$V = V_{of} + V_E + V_c \tag{76}$$

Taking the derivative of (76), and combining (23), (56), and (75), we can obtain

$$\begin{aligned} \dot{V} &\leq -c_1\bar{c}_0V_{of}^\varepsilon - [c_1(1 - \bar{c}_0)V_{of}^{\varepsilon-1+\frac{\sigma}{2}} - c_0]V_{of}^{1-\frac{\sigma}{2}} \\ &\quad - k_u\hat{u}_e^2 - 2^{\frac{3}{4}}k_{u_1}|\frac{1}{2}\hat{u}_e|^{\frac{3}{4}} - \frac{1}{2}k_{smin}\|\mathbf{E}\|^2 \\ &\quad - k_r\hat{r}_e^2 - 2^{\frac{3}{4}}k_{r_1}|\frac{1}{2}\hat{r}_e|^{\frac{3}{4}} - k_{\zeta\beta_1}\hat{\zeta}_\beta^2 - 2^{\frac{3}{4}}k_{\zeta\beta_2}|\frac{1}{2}\hat{\zeta}_\beta|^{\frac{3}{4}} \\ &\leq -c_1\bar{c}_0V_{of}^\varepsilon - [c_1(1 - \bar{c}_0)V_{of}^{\varepsilon-1+\frac{\sigma}{2}} - c_0]V_{of}^{1-\frac{\sigma}{2}} - k_{s_1}V_E \\ &\quad - k_{c_1}V_c - k_{c_2}V_c^{\frac{3}{4}} \end{aligned} \tag{77}$$

where  $k_{c_1} = \{k_u, k_r, k_{\zeta\beta}\}$  and  $k_{c_2} = \min\{2^{\frac{3}{4}}k_{u_1}, 2^{\frac{3}{4}}k_{r_1}, 2^{\frac{3}{4}}k_{\zeta\beta_1}\}$ .

According to (77), when the following inequality  $V_{of}^{\varepsilon-1+\frac{\sigma}{2}} > \frac{c_0}{c_1(1-\bar{c}_0)}$  holds,

$$\dot{V} \leq -k_{s_1}V_E - k_cV_c \leq -k_\rho V \tag{78}$$

where  $k_\rho = \min\{k_{s_1}, k_c\}$ .

Hence,

$$0 \leq V \leq V(0)e^{-k_\rho t} \tag{79}$$

It is obvious that the Lyapunov function  $V_{of}$  of the closed-loop system is bounded, and errors  $\omega, x_e, y_e, \hat{u}_e, \hat{r}_e$  are uniformly bounded.

Subsequently, the proof of finite-time convergence will be analyzed. We can see from Theorem 1 that the observation error of FTESO can converge to zero, i.e.,  $\hat{\boldsymbol{\mu}} = \boldsymbol{\mu}$ .

Since position tracking errors  $x_e, y_e$  are bounded, the hovercraft's position is bounded. Similarly,  $u_d$  is constant and  $\hat{u}_e = \hat{u} - u_d, \hat{r}_e = \hat{r} - r_d$  are bounded; thus,  $\hat{u}, \hat{r}$  are bounded.  $S(\psi)$  and  $\tilde{\boldsymbol{\mu}} = \hat{\boldsymbol{\mu}} - \boldsymbol{\mu}$  are also bounded at the same time. In addition, the sway velocity is bounded according to previous research.  $\square$

**Remark 5.** The FTESO can achieve the estimated performance of lumped disturbances containing the model and external uncertainties in finite time, and the errors' convergence is faster than infinite. As a result, the constructed robust, nonlinear control scheme has a better performance.

### 5. Numerical Simulations

In this section, numerical simulations are executed to prove the presented method's efficiency demonstrated on a hovercraft in this paper. Firstly, the nomenclature of a hovercraft is depicted in Table 1 [36].

**Table 1.** Nomenclature.

Parameter	Value	Unit	Parameter	Value	Unit
$m_0$	40,000	kg	$J_{z0}$	$1.8 \times 10^6$	$\text{kg}\cdot\text{m}^2$
$J_{x0}$	$2.5 \times 10^5$	$\text{kg}\cdot\text{m}^2$	$S_{PP}$	45	$\text{m}^2$
$S_{LP}$	93	$\text{m}^2$	$S_{HP}$	260	$\text{m}^2$
$Q$	140.8	$\text{m}^3/\text{s}$	$S_c$	212	$\text{m}^2$
$l_{sk}$	65	m	$B_c$	8.9	m
$h_m$	2.4	m	$l_c$	23.6	m
$h$	1	m	$H_{hov}$	5.9	m
$V_w$	5	knot	$\beta_w$	45	deg

The initial values of a hovercraft satisfying Assumption 2 are as follows:

$$u(0) = 30, v(0) = 0, r(0) = 0, \text{ and } \beta(0) = 0.$$

Main hovercraft parameters are as follows:  $x(0) = -500, y(0) = 200$ , and  $-2 \leq \beta \leq 2$ . The starting pose of the generated parameterized reference line path follows  $x(0) = -500$

and  $y(0) = 200$ , and the ending pose is plotted in Figure 4. The lumped disturbances [37] are described as follows:

$$\begin{aligned} d_u &= 2 \sin(0.05t) / m_0 * b_1 \\ d_v &= 0.2 \cos(0.03t) / m_0 * b_2 \\ d_r &= \cos(0.02t) / J_{z0} * b_3 \end{aligned} \tag{80}$$

where  $\mathbf{b} = [b_1 \ b_2 \ b_3]^T$  and  $\dot{\mathbf{b}} = -\mathbf{T}^{-1}\mathbf{b} + \mathbf{A}\mathbf{w}_n$  are the first-order Markov process and the vector of zero-mean Gaussian white noise, respectively; the other parameters of the first-order Markov process are set as follows:

$$\mathbf{b}(0) = [2 \times 10^4, \ 2 \times 10^4, \ 2 \times 10^4]^T, \ \mathbf{T} = \text{diag}(10^3, 10^3, 10^3), \ \mathbf{A} = \text{diag}(1 \times 10^4, \ 1 \times 10^4, \ 1 \times 10^4)$$

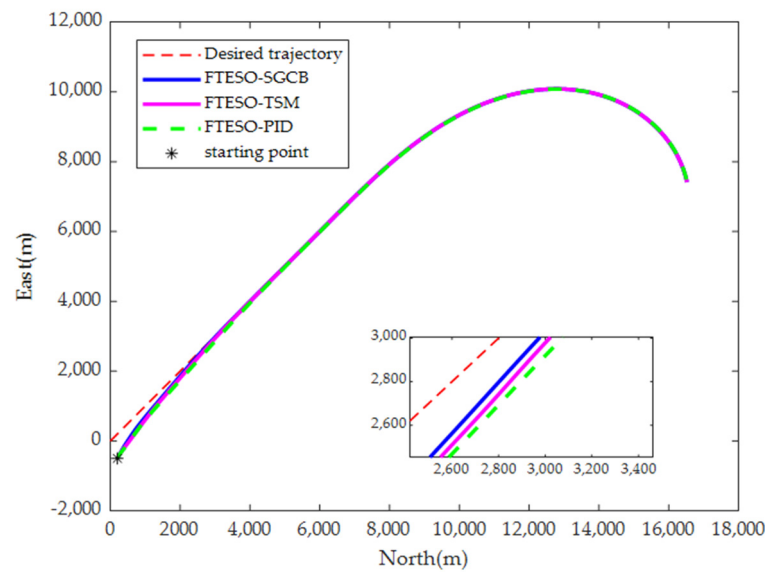


Figure 4. Path of the hovercraft.

In order to indicate the advantage and validity of the proposed safety-guaranteed, robust, nonlinear controller with FTESO, numerical simulation results are executed to compare the PID and TSM’s performances.

The PID controller based on the feedback error is designed as follows:

$$\begin{cases} e_u = u - \alpha_u \\ \tau_p = k_{p1}e_u + k_{d1}\dot{e}_u + k_{i1}\int_0^t e_u dt \\ e_v = v - \alpha_v \\ \alpha_v = k_{p2}e_v + k_{d2}\dot{e}_v + k_{i2}\int_0^t e_v dt \\ e_r = r - \alpha_r \\ \tau_R = k_{p3}e_r + k_{d3}\dot{e}_r + k_{i3}\int_0^t e_r dt \end{cases} \tag{81}$$

where the design parameters are set as  $k_{p1} = 1.6$ ,  $k_{d1} = 0.5$ ,  $k_{i1} = 0.08$ ,  $k_{p2} = 0.35$ ,  $k_{d2} = 0.5$ ,  $k_{i2} = 0.001$ ,  $k_{p3} = 0.4$ ,  $k_{d3} = 4.2$ , and  $k_{i3} = 0.001$  according to previous engineering experience.

The TSM controller based on the feedback error is designed as follows:

$$\left\{ \begin{array}{l} s_u = \dot{e}_u + c_u e_u^{q_u/p_u} \\ \tau_p = m_0(-vr - \frac{1}{m_0} F_{xD0}) - c_u e_u^{q_u/p_u} + \dot{\alpha}_u \\ \dot{\tau}_{Ps} = -\eta_u \text{sign}(s_u) \\ s_v = \dot{e}_v + c_v e_v \\ \alpha_r = -\frac{1}{u}(-\frac{F_{xD0}}{m_0} - c_v e_v + \dot{\alpha}_u - \eta_v s_v) \\ s_r = \dot{e}_r + c_r e_r^{q_r/p_r} \\ \tau_R = J_{z0}(-\frac{M_{zD0}}{J_{z0}} - c_r e_r^{q_r/p_r} + \dot{\alpha}_r) \\ \dot{\tau}_{Rs} = -\eta_r \text{sign}(s_r) \end{array} \right. \quad (82)$$

where the design parameters are  $c_u = 2$ ,  $\eta_u = 1.1$ ,  $q_u/p_u = 7/8.9$ ,  $c_v = 0.35$ ,  $\eta_v = 0.6$ ,  $c_r = 1$ ,  $\eta_r = 1.1$ , and  $q_r/p_r = 7/8.9$ .

The proposed controller design parameters and the FTESO's parameters are designed as follows:  $\chi = \delta_s = 6$ ,  $k_{s1} = 0.03$ ,  $\Delta = 20$ ,  $k_\psi = 6$ ,  $k_{\psi1} = 0.001$ ,  $k_r = 6$ ,  $k_{r1} = 0.001$ ,  $l_1 = 0.85$ ,  $l_2 = 0.8$ ,  $l_3 = 0.03$ ,  $\lambda_1 = 0.05$ ,  $\lambda_2 = 0.05$ ,  $\lambda_3 = 0.0003$ . The parameters of the auxiliary system are selected as follows:  $k_{\zeta\beta_1} = 3.1$ ,  $k_{\zeta\beta_2} = 0.1$ ,  $k_{\zeta\beta_3} = 0.02$ ,  $k_\beta = 1.2$ ,  $\delta = 0.00001$ .

The simulation results and comparisons are presented by different lines in Figures 4–8. It can be seen from Figure 4 and Table 2 that three control strategies ensure that the hovercraft follows the desired path with high performance, and the FTESO-based, safety-guaranteed compensation backstepping (FTESO-SGCB) method performs better than the FTESO-based PID (FTESO-PID) and the FTESO-based TSM (FTESO-TSM) methods under the model uncertainties and external ocean disturbances. With the adjustment of the controllers in three situations, they all can approach the generated desired path and follow the virtual hovercraft's motion. It can be seen from Figure 5 and Table 2 that the controller proposed is effective and guarantees that whether following a straight line or a quasi-circle path, all error signals can converge to an arbitrarily small region near the origin within finite time and the presented controllers have faster convergence speed, higher tracking accuracy, and stronger robustness than the PID controller and the TSM controller. The curves of the sway velocity and yaw angular velocity during navigation are shown in Figure 6a. It is worth noting that the drift angle is restrained to stay within safety limits in real-time under the proposed controllers in Figure 6a. The control inputs are presented in Figure 6b. Figure 7a shows that the hovercraft's velocities can track the expected velocity generated by the three relative controllers, whereas the convergence time of the proposed control scheme is shorter than those of the other two. The yaw angle and reference yaw angle are displayed in Figure 7b. The uncertainties and the corresponding estimation values are depicted in Figure 8. All shown simulations and comparisons illustrate the superiority and robustness of the proposed method.

Under the action of the three controllers, the control accuracy range of the position tracking error between 300 s and 700 s, and the tracking errors, are depicted in Table 2. The proposed method performs better than the FTESO-based PID (FTESO-PID) and the FTESO-based TSM (FTESO-TSM) methods under the model uncertainties and external ocean disturbances. The proposed controller has the highest control accuracy and the error under is ultimately within the range of 0.30 m, 0.20 m, 0.01 knots, 0.04 knots, and 0.004 deg/s.

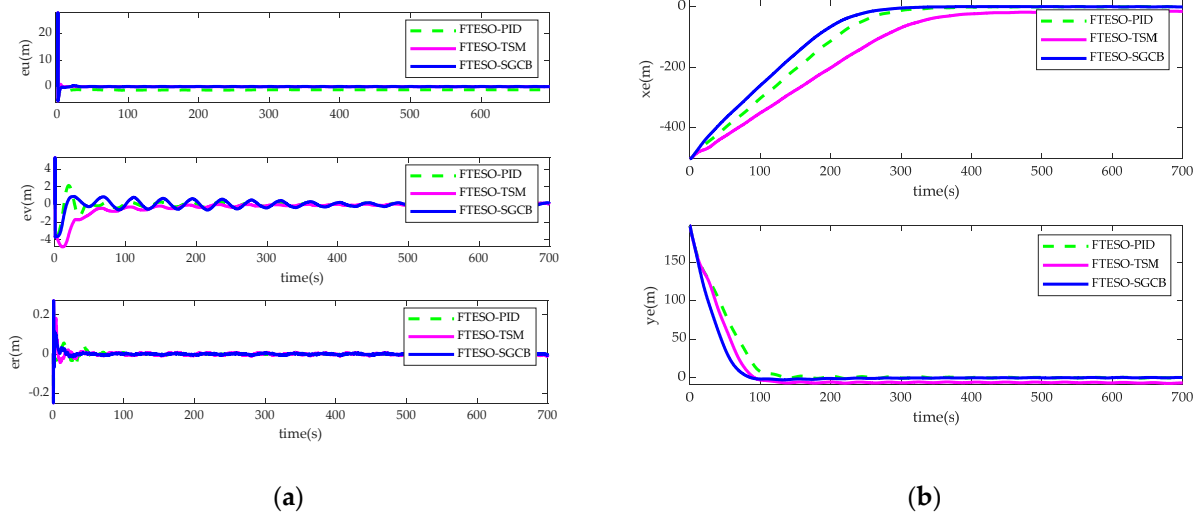


Figure 5. (a) Tracking errors. (b) Along-track  $x_e$  and cross-track  $y_e$  errors.

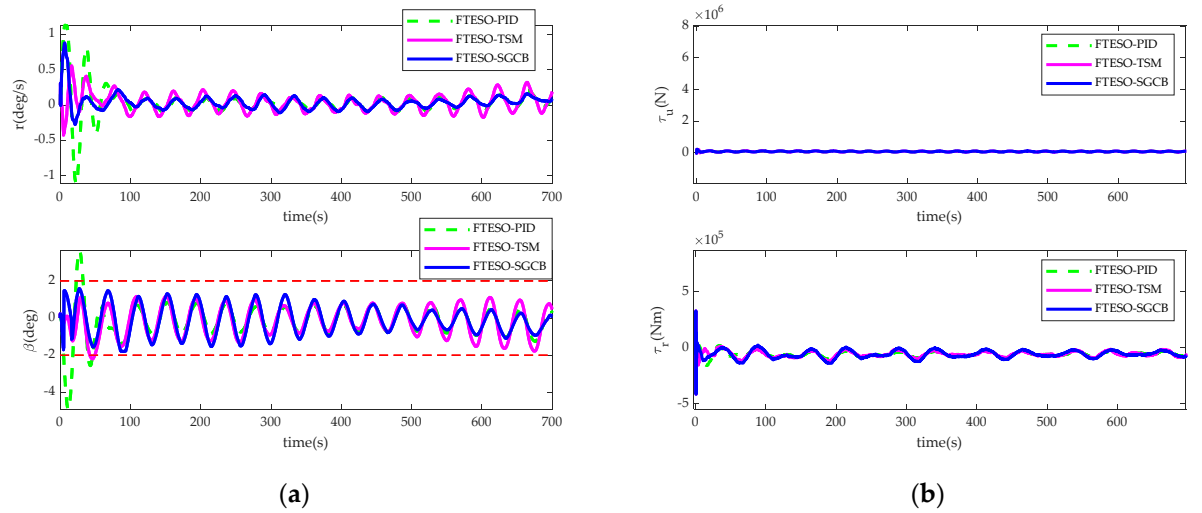


Figure 6. (a) Rate of turning and drift angle of the hovercraft. (b) The control inputs  $\tau_u, \tau_r$ .

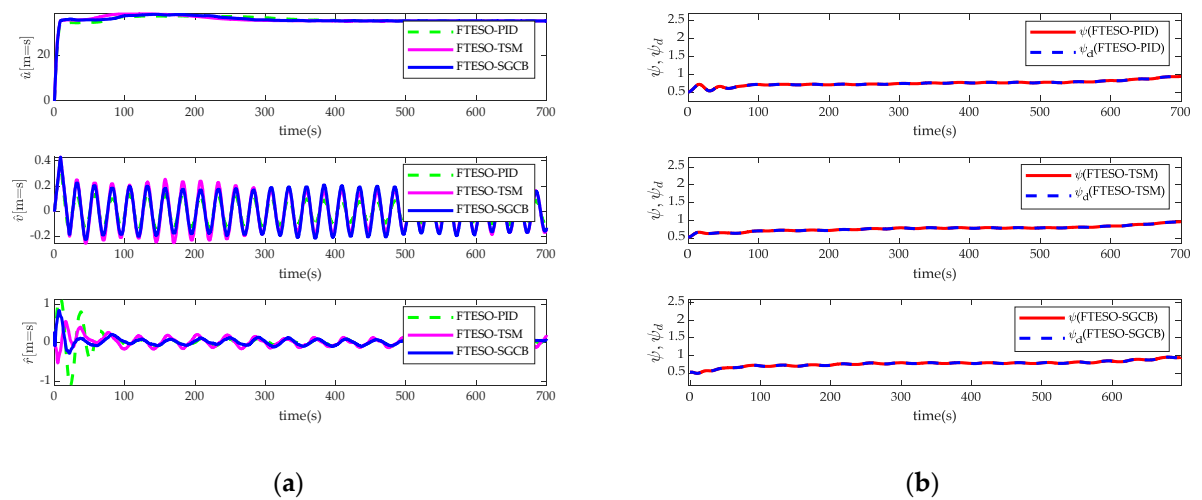


Figure 7. (a) The observation of  $u, v, r$ . (b) Yaw angle  $\psi$  and reference yaw angle  $\psi_d$ .

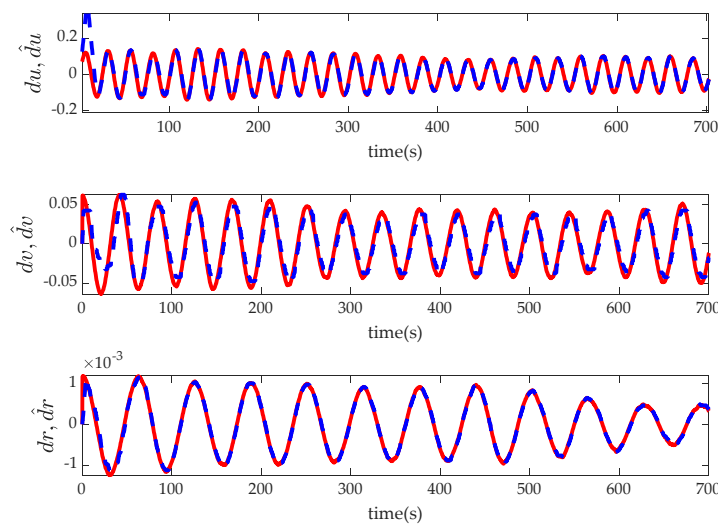


Figure 8. Estimation performance of the proposed observer.

Table 2. Control accuracy of four different controllers.

Controller	$ x_e (m)$	$ y_e (m)$	$ e_u (knots)$	$ e_v (knots)$	$ e_r (deg/s)$
FTESO-PID	$\leq 0.60$	$\leq 0.50$	$\leq 1.10$	$\leq 0.25$	$\leq 0.05$
FTESO-TSM	$\leq 5.40$	$\leq 3.80$	$\leq 0.05$	$\leq 0.14$	$\leq 0.01$
FTESO-SGCB	$\leq 0.30$	$\leq 0.20$	$\leq 0.01$	$\leq 0.04$	$\leq 0.004$

## 6. Conclusions

In this paper, the safety-guaranteed, robust, nonlinear controller with FTESO is constructed for a hovercraft with unavailable velocity, unknown uncertainties containing the model, and external disturbances. The presented FTESO has been introduced to observe the unavailable velocities and unknown disturbances while converging to zero within finite time via the homogeneous theory; according to a line-of-sight (LOS) guidance law via the bounded-gain-forgetting (BGF) adaptive estimator, our method can obtain the reference yaw angle law and meet the requirement of finite time convergence. The proposed controllers can handle the problems of strong nonlinearity and complex model uncertainties for a hovercraft by combining with the observer. The safety-guaranteed auxiliary system can restrict the drift angle to be more stably constrained to the inside of the safety boundary, varying with time. Finally, the simulation results and comparisons have demonstrated the efficiency of the presented control scheme. In future works, the proposed method may be extended to a hovercraft model with four degrees of freedom while considering various safety constraints. Additionally, the proposed method may be utilized in a safety-guaranteed control formation plan with other performance standards required for autonomous surface vessels; this will be considered in future research.

**Author Contributions:** M.F., methodology, investigation, funding acquisition, project administration; Q.W., investigation, writing—original draft, software, data curation. All authors have read and agreed to the published version of the manuscript.

**Funding:** This research was funded by National Natural Science Foundation of China, grant numbers 52071112 and 51309062; Fundamental Research Funds for the Central Universities, grant number 3072020CF0408.

**Institutional Review Board Statement:** Not applicable.

**Informed Consent Statement:** Not applicable.

**Data Availability Statement:** The original data contributions presented in the study are included in the article; further inquiries can be directed to the corresponding authors.

**Conflicts of Interest:** The authors declare no conflict of interest.

## References

1. Fu, M.; Zhang, T.; Ding, F.; Wang, D. Safety-guaranteed adaptive neural motion control for a hovercraft with multiple constraints. *Ocean Eng.* **2020**, *220*, 108401. [[CrossRef](#)]
2. Hua, F. Analysis and consideration on safety of all-lift hovercraft. *Ship Boat* **2008**, *6*, 1–3.
3. Fu, M.; Gao, S.; Wang, C.; Li, M. Design of driver assistance system for air cushion vehicle with uncertainty based on model knowledge neural network. *Ocean Eng.* **2019**, *172*, 296–307. [[CrossRef](#)]
4. Rigatos, G.G.; Raffo, G.V. Input–Output Linearizing Control of the Underactuated Hovercraft Using the Derivative-Free Nonlinear Kalman Filter. *Unmanned Syst.* **2015**, *3*, 127–142. [[CrossRef](#)]
5. Morales, R.; Sira-Ramírez, H.; Somolinos, J.A. Linear active disturbance rejection control of the hovercraft vessel model. *Ocean Eng.* **2015**, *96*, 100–108. [[CrossRef](#)]
6. Shojaei, K. Neural adaptive robust control of underactuated marine surface vehicles with input saturation. *Appl. Ocean Res.* **2015**, *53*, 267–278. [[CrossRef](#)]
7. Fu, M.; Zhang, T.; Ding, F. Adaptive Safety Motion Control for Underactuated Hovercraft Using Improved Integral Barrier Lyapunov Function. *Int. J. Control Autom. Syst.* **2021**, *19*, 2784–2796. [[CrossRef](#)]
8. Gao, S.; Xue, J. Nonlinear vector model control of underactuated air cushion vehicle based on parameter reduction algorithm. *Trans. Inst. Meas. Control* **2020**, *43*, 1202–1211. [[CrossRef](#)]
9. Sun, Z.; Zhang, G.; Yang, J.; Zhang, W. Research on the sliding mode control for underactuated surface vessels via parameter estimation. *Nonlinear Dyn.* **2018**, *91*, 1163–1175. [[CrossRef](#)]
10. Lu, Y.; Zhang, G.; Sun, Z.; Zhang, W. Robust adaptive formation control of underactuated autonomous surface vessels based on MLP and DOB. *Nonlinear Dyn.* **2018**, *94*, 1–17. [[CrossRef](#)]
11. Wu, M.; Liu, L.; Yu, Z. Augmented safety guarantee-based area keeping control for an underactuated USV with environmental disturbances. *ISA Trans.* **2021**, *127*, 415–422. [[CrossRef](#)]
12. Gao, S.; Peng, Z.; Liu, L.; Wang, H.; Wang, D. Coordinated target tracking by multiple unmanned surface vehicles with communication delays based on a distributed event-triggered extended state observer. *Ocean Eng.* **2021**, *227*, 108283. [[CrossRef](#)]
13. Woo, J.; Yu, C.; Kim, N. Deep reinforcement learning-based controller for path following of an unmanned surface vehicle. *Ocean Eng.* **2019**, *183*, 155–166. [[CrossRef](#)]
14. Harshavarthini, S.; Sakthivel, R.; Ahn, C.K. Finite-time reliable attitude tracking control design for nonlinear quadrotor model with actuator faults. *Nonlinear Dyn.* **2019**, *96*, 2681–2692. [[CrossRef](#)]
15. Zong, G.; Ren, H.; Karimi, H.R. Event-Triggered Communication and Annular Finite-Time  $H_\infty$  Filtering for Networked Switched Systems. *IEEE Trans. Cybern.* **2020**, *51*, 309–317.
16. Sun, K.; Qiu, J.; Karimi, H.R.; Fu, Y. Event-Triggered Robust Fuzzy Adaptive Finite-Time Control of Nonlinear Systems With Prescribed Performance. *IEEE Trans. Fuzzy Syst.* **2020**, *29*, 1460–1471. [[CrossRef](#)]
17. Nie, J.; Lin, X. FAILOS guidance law based adaptive fuzzy finite-time path following control for underactuated MSV. *Ocean Eng.* **2019**, *195*, 106726. [[CrossRef](#)]
18. Wang, N.; Sun, Z.; Jiao, Y.; Han, G. Surge-Heading Guidance Based Finite-Time Path-Following of Underactuated Marine Vehicles. *IEEE Trans. Veh. Technol.* **2019**, *68*, 8523–8532. [[CrossRef](#)]
19. Wang, N.; Ahn, C.K. Hyperbolic-Tangent LOS Guidance-Based Finite-Time Path Following of Underactuated Marine Vehicles. *IEEE Trans. Ind. Electron.* **2019**, *67*, 8566–8575. [[CrossRef](#)]
20. Nie, J.; Wang, H.; Lu, X.; Lin, X.; Sheng, C.; Zhang, Z.; Song, S. Finite-time output feedback path following control of underactuated MSV based on FTESO. *Ocean Eng.* **2021**, *224*, 108660. [[CrossRef](#)]
21. Wang, Y.; Tong, H.; Fu, M. Line-of-sight guidance law for path following of amphibious hovercrafts with big and time-varying sideslip compensation. *Ocean Eng.* **2019**, *172*, 531–540. [[CrossRef](#)]
22. Nakamura, H.; Yamashita, Y.; Nishitani, H. Smooth Lyapunov functions for homogeneous differential inclusions. In Proceedings of the 41st SICE Annual Conference, Osaka, Japan, 5–7 August 2002; pp. 1974–1979.
23. Song, Z.; Li, H.; Sun, K. Finite-time control for nonlinear spacecraft attitude based on terminal sliding mode technique. *ISA Trans.* **2013**, *53*, 117–124. [[CrossRef](#)] [[PubMed](#)]
24. Hardy, G.H.; Littlewood, J.E.; Pólya, G. *Inequalities (Cambridge Mathematical Library)*; Cambridge University Press: Cambridge, UK, 1934.
25. Zou, A.M.; De Ruiter, A.H.J.; Kumar, K.D. Distributed finite-time velocity-free attitude coordination control for spacecraft formations. *Automatica* **2016**, *67*, 46–53. [[CrossRef](#)]
26. Cohen, M.; Miloh, T.; Zilman, G. Wave resistance of a hovercraft moving in water with nonrigid bottom. *Ocean Eng.* **2001**, *28*, 1461–1478. [[CrossRef](#)]
27. Tao, M.; Chengjie, W. *Hovorcrafft Performance and Skirt-Cushion System Dynamics Design*; National Defense Industry Press: Beijing, China, 2012.

28. Peng, Z.; Wang, D.; Chen, Z.; Hu, X.; Lan, W. Adaptive Dynamic Surface Control for Formations of Autonomous Surface Vehicles With Uncertain Dynamics. *IEEE Trans. Control Syst. Technol.* **2013**, *21*, 513–520. [[CrossRef](#)]
29. Perruquetti, W.; Floquet, T.; Moulay, E. Finite-Time Observers: Application to Secure Communication. *IEEE Trans. Autom. Control* **2008**, *53*, 356–360. [[CrossRef](#)]
30. Adetola, V.; Guay, M. Performance improvement in adaptive control of linearly parameterized nonlinear systems. *IEEE Trans. Autom. Control* **2010**, *55*, 2182–2186. [[CrossRef](#)]
31. Dhaliwal, S.; Guay, M. Set-based adaptive estimation for a class of nonlinear systems with time-varying parameters. *Adv. Control Chem. Process.* **2012**, *45*, 391–395. [[CrossRef](#)]
32. Adetola, V.; Guay, M. Robust adaptive MPC for systems with exogeneous disturbances. *IFAC Int. Symp. Adv. Control Chem. Process.* **2009**, *42*, 249–254.
33. Pomet, J.-B.; Praly, L. Adaptive nonlinear regulation: Estimation from the Lyapunov equation. *IEEE Trans. Autom. Control* **1992**, *37*, 729–740. [[CrossRef](#)]
34. Liu, L.; Wang, D.; Peng, Z. ESO-based line-of-sight guidance law for path following of underactuated marine surface vehicles with exact sideslip compensation. *IEEE J. Ocean. Eng.* **2017**, *42*, 477–487. [[CrossRef](#)]
35. Chen, M.; Ge, S.S.; Ren, B. Adaptive tracking control of uncertain MIMO nonlinear systems with input constraints. *Automatica* **2011**, *47*, 452–465. [[CrossRef](#)]
36. Fu, M.; Gao, S.; Wang, C.; Li, M. Human-centered Automatic Tracking System for Underactuated Hovercraft Based on Adaptive Chattering-free Full-order Terminal Sliding Mode Control. *IEEE Access* **2018**, *6*, 37883–37892. [[CrossRef](#)]
37. Du, J.; Hu, X.; Krstić, M.; Sun, Y. Robust dynamic positioning of ships with disturbances under input saturation. *Automatica* **2016**, *73*, 207–214. [[CrossRef](#)]

**Disclaimer/Publisher’s Note:** The statements, opinions and data contained in all publications are solely those of the individual author(s) and contributor(s) and not of MDPI and/or the editor(s). MDPI and/or the editor(s) disclaim responsibility for any injury to people or property resulting from any ideas, methods, instructions or products referred to in the content.